Available online at www.sciencedirect.com
SCIENCE DIRECT
Wear 260 (2006) 433–437
WEAR
www.elsevier.com/locate/wear

Structure and mechanical properties of tribologically induced nanolayers

D. Shakhvorostov, K. Pöhlmann, M. Scherge *

IAVF Antriebstechnik AG, Im Schlehert 32, D-76187 Karlsruhe, Germany

Received 12 July 2004; received in revised form 22 January 2005; accepted 15 February 2005
Available online 29 April 2005

Abstract

Ultra low wear rates are common for lubricated state-of-the-art mechanical devices used in machines and cars. The main paths of energy dissipation are heat and wear generation as well as a significant change of near-surface material within the range of a few hundred nanometers. Due to mechanical intermixing at the asperity level the involved materials change with respect to chemical composition, morphology and mechanical properties. By means of focused ion beam analysis the morphology of the near-surface material of tribologically stressed and unstressed samples was investigated. In addition, nanoindentation was applied to characterize the mechanical properties. In the presented study mechanical intermixing leads to nanocrystalline material which is softer than bulk material. Depending on the level of tribological stressing, the modified material exhibits smaller energy dissipation, thus lower friction and wear.

Keywords: Wear mechanisms; Nanomechanics

1. Introduction

To classify the level of tribological interaction the total dissipated power $\dot{E}_{\text{tot}}$ expressed as:

$$\dot{E}_{\text{tot}} = \mu F_{\text{n}} v \tag{1}$$

is an effective tool. F_{n} is the normal force, v the sliding velocity and μ is the coefficient of friction. Whereas F_{n} and v are considered as experimental input values, μ represents the reaction of the system. The coefficient of friction is influenced by the joint response of both solids, the lubricant and the environment. In addition, the running-in has crucial influence on the evolution of μ. Table 1 shows the attempt of a systematization. Tribological systems are distinguished with respect to Eq. (1) leading to four categories termed as nano, micro, meso and macro. In total the dissipated power covers a range from 10^{-16} to 10^{2} W. For each category a typical technical application was added.

In this study optimized macrotribological systems are in focus. Due to high loads and large sliding velocities the pressure an asperity has to carry is frequently larger than the yield stress of the material. As a result, the asperities start to flow leading to an indiscriminate mixture of asperity, counter-asperity and lubricant. This process is called mechanical intermixing [1]. Since this process occurs simultaneously at thousands of asperities, the whole contact area is subject to a step-wise intermixing accompanied by the introduction of foreign elements. As a result of the intermixing a modified zone with a thickness between 10 nm and several hundred nanometers can evolve where the thickness is a function of the amount of energy dissipated in the microcontacts. Taking Bowden and Tabor's model [2]:

$$F_{\text{f}} = \tau A_{\text{c}}, \tag{2}$$

where τ is the material dependent shear coefficient representing the combined response of both (flowed) solids and the lubricant. A_{c} is the real contact area. Eq. (2) represents the friction force of a single asperity contact. When a system is adequately stressed friction decreases throughout the ex-

* Corresponding author. Tel.: +49 721 95505 30; fax: +49 721 95505 44.
E-mail address: matthias.scherge@iavf.de (M. Scherge).

0043-1648/$ – see front matter © 2005 Elsevier B.V. All rights reserved.
doi:10.1016/j.wear.2005.02.086

Table 1
Dissipated power and typical application

Scale	Nano	Micro	Meso	Macro
Power (W)	10^{-16}–10^{-13}	10^{-13}–10^{-5}	10^{-5}–10^{-2}	10^{-2}–10^{2}
Application	Nano machines	MEMS	Computer hard drive	Engines, gears

periment due to decreasing τ. This in turn means that both materials can be sheared more easily, i.e., by consuming less energy.

After proper material and lubricant selection as well as adequate running-in sliding friction of metallic contacts is usually accompanied by mild wear. If the wear rate is expressed as length versus time, then the materials wear with rates in the range of some nanometers per hour. Stimulated by this hypothesis, the crystalline properties and the mechanical response of materials before and after tribological stressing were determined. Using focused ion beam analysis the grain structure was made visible. Nanoindentation was used to measure nanohardness.

2. Experimental details

2.1. Test procedure

A common pin-on-disk tribometer was used to generate the samples. In all experiments a chromium-plated steel pin with a diameter of 3 mm was run against a gray cast iron disk with lubrication (Fuchs Titan 5W40). The disk was cut from a cast iron cylinder, turned and surface finished (Supfina). The oscillating finishing stone was frontally pressed against the slowly rotating disk. Wear was measured with the radionuclide technique [3] allowing real-time tests to monitor the wear rate with a resolution of some nanometers per hour. In a series of screening experiments prior to the data published here the normal forces ranged between 100 and 550 N and the sliding velocities were varied between 1 to 10 m/s. Out of a variety of possible combinations two representative examples were selected to illustrate different tribological states as shown in Table 2.

The tribological state refers to the wear rate at the end of the test after 68 h, see Fig. 1. Both normal force and sliding velocity were kept constant throughout the test. To calculate $\dot{E}_{tot}$ an average coefficient of friction was applied to Eq. (1). The large fluctuations in total dissipated power arise from the impact of the coefficient of friction as response of the system [4]. When a system runs in properly both the coefficient of friction and the wear rate quickly adopt stable and low values. Many tests showed that optimum values can be achieved when the system is subjected to high but not too high values of normal force and sliding velocity (sample B) [5]. This statement is weak. However, it underlines the role of continuous wear measurement in real-time. If the interaction is too intense (sample C) the system responds with high wear and eventually switches to severe wear. This behavior explains why the total dissipated power shows clearly different values.

Table 2
Sample selection and stressing conditions

Sample	Tribological state	F_n (N)	v (m/s)	$\dot{E}_{tot}$ (W)
A	Unstressed	–	–	–
B	Fairly run-in	515	2.5	30
C	High wear	515	5.0	230

2.2. Structural analysis

Focused ion beam (FIB) analysis was used to minimize the impact of mechanical pre-treatment to the samples. To analyze the material in the intermixed zone, a beam of accelerated Ga ions was used to cut a trench into the gray cast iron surface, see Fig. 2. The fundamental principle of the applied FIB system resembles that of a scanning electron microscope. The main difference exists in the use of accelerated gallium ions (Ga^+) instead of an electron beam. The ion beam is produced in a liquid metal ion gun and accelerated in a strong electrical field. At low energy, an image of the surface was generated by secondary electrons. Fig. 2 shows that the surface of the sample was protected by a tungsten shield to prevent the topmost material from mechanical intermixing upon contact with the ions. One side of the trench was cut perpendicular to the surface whereas the opposite side was prepared in steps as demonstrated in the lower part of Fig. 2.

2.3. Mechanical analysis

Nanoindentation was applied for measuring the mechanical properties at very small length scales appropriate to the depth of the intermixed zone. The analysis involved the simul-

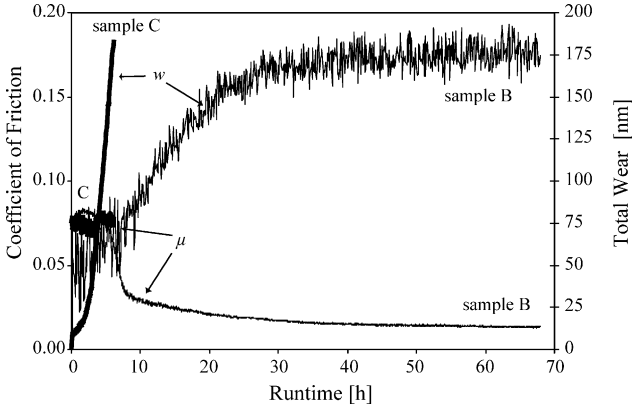

Fig. 1. Friction and wear curves of samples B and C.

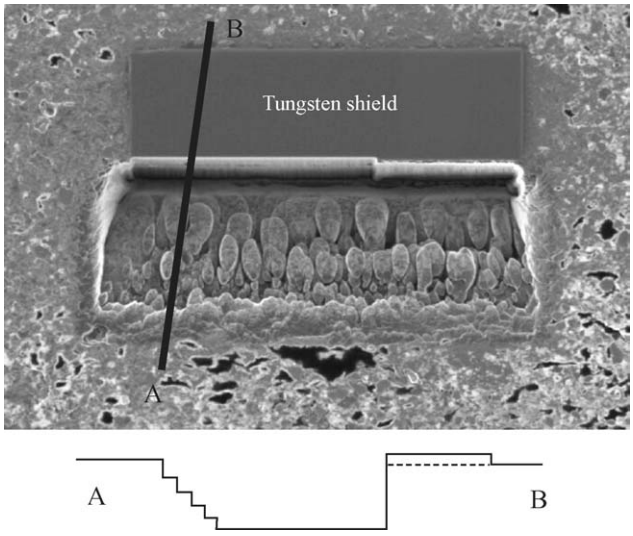

Fig. 2. Focused ion beam analysis and cross section between points A and B.

taneous measurement of contact load and depth of penetration of the indenter tip into the material according to [6]. The lateral resolution of the measurements was determined by the geometry of the Berkovich indenter. For this geometry, the lateral dimension of the contact impression is approximately seven times the depth. All nanoindentation experiments were performed using a Nano Indenter XP (MTS Systems Corporation). Before the test, the samples were cleaned with acetone in an ultrasonic bath and mounted on the sample holder. In the nanoindentation tests, load, depth and contact stiffness were recorded simultaneously for the complete load-unload cycle. Applying the Continuous Stiffness Measurement technique, hardness was measured as a function of depth. Each test was programmed to go to a maximum penetration depth of 1500 nm at constant strain rate. The hardness versus depth information was not polluted by strain-rate effects. The limit of the penetration depth was chosen according to the expected thickness of the modified zone. After reaching the depth limit, the load was held constant for 10 s to eliminate creep effects. A thermal drift correction was done for each test after the indentation by using the information of a second constant load segment at 95% unloading.

3. Results

3.1. Morphology

Fig. 3 shows four FIB sections where the wall perpendicular to the surface is of further interest. In the wall of all three samples the grain structure is clearly visible. Sample A represents the state after surface finish (Fig. 3a). Due to the final grinding process the grain structure appears textured and the individual grains close to the surface are stretched parallel to the surface. The final manufacturing step has already led to a grain size reduction.

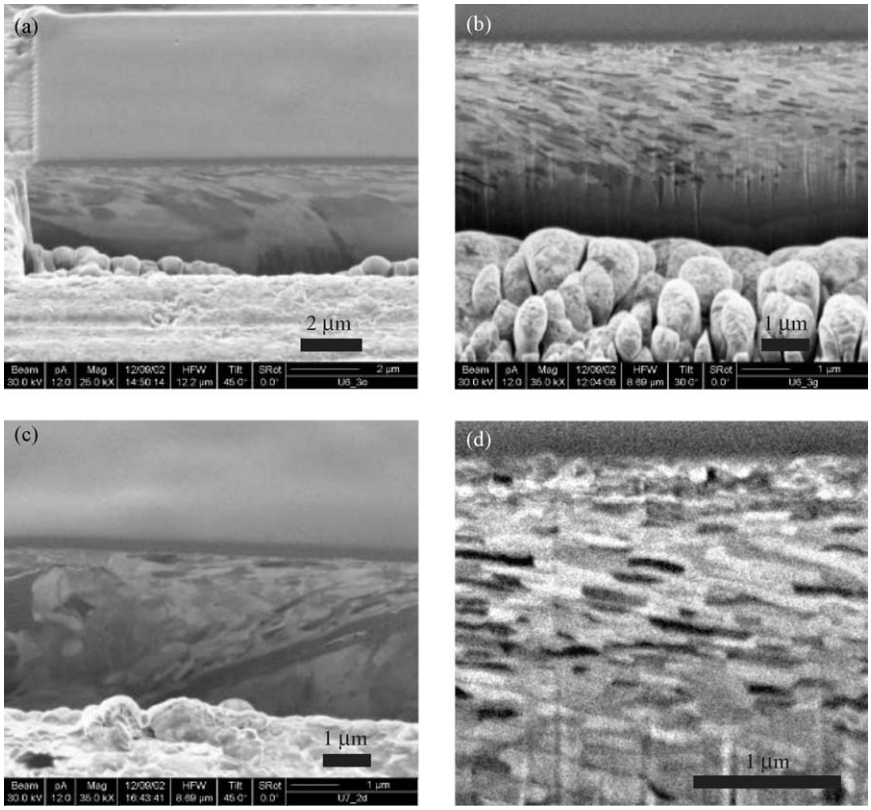

Fig. 3. Focused ion beam analysis. (a) Sample A, (b) and (d) sample B, (c) sample C.

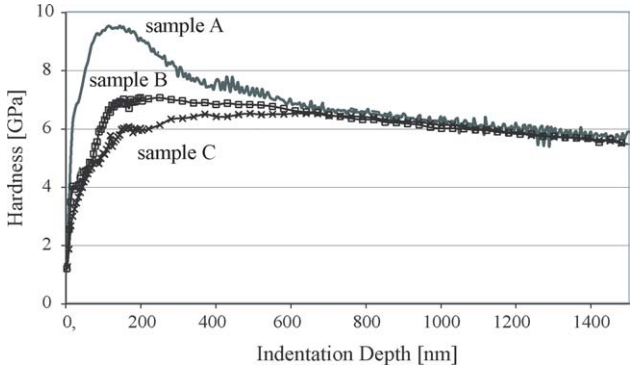

Fig. 4. Nanoindentation of samples A, B and C.

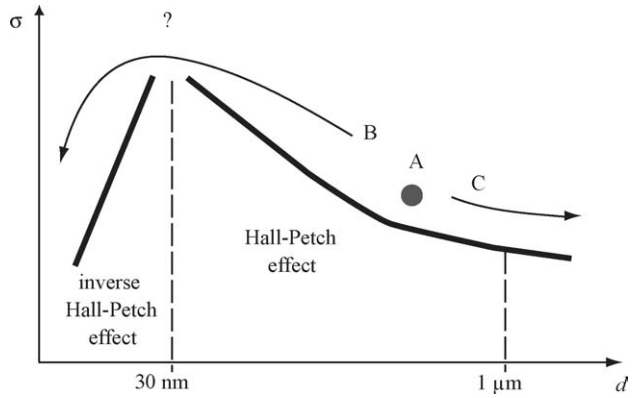

Fig. 5. Qualitative behavior of yield stress as function of grain size [9].

After tribological stressing the texture is still visible, however, the average grain size has decreased further (Fig. 3b). Grain size analysis using image processing software showed that the grains within the first 200 nm from the surface have an average diameter of about 20 nm (Fig. 3d). In deeper areas, the grains stepwise become larger. The fact is also shown in Fig. 2. Starting at point A small grains can be detected. As one proceeds deeper into the trench, the grains become larger. At the bottom of the trench one finds a grain size induced by the surface finish.

At excessively high-dissipated power the appearance of the grain structure changed considerably (Fig. 3c). In contrast to samples A and B no more texturing can been seen. In addition, the grain size increased to values of more than 1 micrometer.

3.2. Mechanical properties

The indentation depth was chosen to probe the material in the range where the FIB analysis showed the tribological impact on the grain size, see Fig. 4. As a result of the surface finish sample A shows increased hardness with a peak at about 175 nm. The surface finish was very gentle but it can be assumed that the grinding process introduced internal stresses and strenghtening due to cold working, leading to higher hardness. Sample B shows significantly lower hardness than sample A. With increasing dissipated power (sample C) the peak vanishes completely, thus the near-surface material becomes gradually softer than the tribologically unstressed material. At a depth of about 700 nm bulk properties were reached and all samples showed the same hardness values.

4. Discussion

The whole discussion centers around the process of plastic flow as result of mechanical interaction at the asperity level. The energy input leads to mixing of both solids and lubricant forming a tribomaterial – the third body [7,8]. The resistance in shearing the formed compound is manifested in the friction force at each individual contact point. Thus, the total friction is the sum of all contributions.

Due to mechanical intermixing the grain size decreases gradually towards a nanocrystalline structure. As it is known from the Hall–Petch effect, the mechanical strength increases with decreasing grain size presumably due to grain boundary strengthening shown schematically in Fig. 5. This could be the reason for increased friction of sample B during the first 2.5 h, see Fig. 1. In the framework of the Bowden–Tabor model τ increases up to a maximum. In the course of the experiment friction decreases to a stationary minimum value. This effect cannot be explained by the Hall–Petch effect anymore.

Experimental reports on deviations from the Hall–Petch effect – beginning at a critical grain size of about 30 nm [9] – suggest that the usual dislocation pile-up mechanism acting at the grain boundaries in coarse-grained materials may not be effective in nanocrystalline materials [10–14]. Numerical simulations suggest that with decreasing grain size dislocation mechanisms cease and grain boundary sliding becomes dominant. In the grain size range between 10 and 15 nm, grain boundary sliding and dislocation gliding were predicted [15]. Experiments performed with transmission electron microscope showed mobile dislocations in grains as small as 50 nm [16]. However, it has to be underlined that up to now the mechanical behavior of nanocrystalline grains is only poorly understood. Furthermore, most of the experimental results come from tests with pure materials. Returning to the Bowden–Tabor model the inverse Hall–Petch effect suggests that τ has to decrease, because shearing the formed compound becomes gradually easier. When the dissipated power is too large – as for sample C – material also becomes softer. Fig. 3 shows significantly enlarged grains for sample C. Due to high power the grain structure recrystallizes. As a consequence of the Hall–Petch effect-gliding processes can be initiated easier because the material has fewer grain boundaries, see Fig. 5.

Besides the explanation using the Hall–Petch effect the action of the oil additives must also be considered. During running-in the highest amount of power is dissipated. This is the range where the anti-wear additives are supposed to act. Martin et al. point out that upon formation of a tribo-film friction is increased first due to chemical reactions with surface

oxides and drops by almost an order of magnitude in the latter course [17]. The subsequent decrease of friction, however, cannot be explained so far. Depth profiles have shown that due to mechanical intermixing foreign elements are brought into the near-surface volume up to a depth of several hundred nanometers as indicated in the indentation and FIB measurements, see also [5]. It is highly possible that not only the stoichiometry but also the chemical composition change. At this stage it cannot be ruled out that softer materials form by chemical reaction. In addition, there is also no explanation why for proper running-in conditions – where μ increases first before it drops down considerably – the material becomes harder before softening leads to lower friction.

5. Summary

Adequate energy input due to tribological stressing leads to nanocrystalline structure in the near-surface region of the metals. This effect only occurs when an optimized amount of energy is fed into the system. The appropriate tool to control this process is continuous wear measurement based on the radionuclide technique. By monitoring the wear rate the energy input can be controlled in real-time. If the dissipated power is too low, mechanical intermixing cannot be evoked. At too high power the material responds with grain growth due to recrystallization.

References

[1] D.A. Rigney, Transfer, mixing and associated chemical and mechanical processes during the sliding of ductile materials, Wear 245 (2000) 1–9.
[2] F.P. Bowden, D. Tabor, Friction and lubrication, John Wiley and Sons, 1956.
[3] M. Scherge, K. Pöhlmann, A. Gervé, Wear measurement using radionuclide-technique (RNT), Wear 254 (9) (2003) 801–818.
[4] D. Chakhvorostov, K. Pöhlmann, M. Scherge, Simultaneous measurement of friction, wear and temperature, Wear 257 (1–2) (2004) 124–130.
[5] M. Scherge, D. Chakhvorostov, K. Pöhlmann, Fundamental wear mechanism of metals, Wear 255 (1–6) (2003) 395–400.
[6] W. Oliver, G. Pharr, An improved technique for determining hardness and elastic modulus using load and displacement sensing indentation experiments, J. Mater. Res. 7 (1992) 1564–1583.
[7] E. Rabinowicz, L.A. Dunn, P.G. Russel, A study of abrasive wear under three-body conditions, Wear 4 (1961) 345–355.
[8] E. Rabinowicz, A. Mutis, Effect of abrasive particle size on wear, Wear 8 (1965) 381–390.
[9] E. Arzt, Size effects in materials due to microstructural and dimensional constraints: a comparative review, Acta Mater. 46 (16) (1998) 5611–5626.
[10] J. Schiøtz, F. Di Tolla, K. Jacobsen, Softening of nanocrystalline metals at very small grain sizes, Nature 391 (1998) 561.
[11] K. Lu, W. Wei, J. Wang, Microhardness and fracture properties of nanocrystalline Ni–P alloy, Scripta Metall. Mater. 24 (1990) 2319–2323.
[12] G. Fougere, J. Weertman, R. Siegel, Grain-size dependent hardening and softening of nanocrystalline Cu and Pd, Scripta Metall. Mater. 26 (1992) 1879–1883.
[13] H. Conrad, J. Narayan, On the grain size softening in nanocrystalline materials, Scripta Mater. 42 (2000) 1025–1030.
[14] B. Cai, Q. Kong, L. Lu, K. Lu, Interface controlled diffusional creep of nanocrystalline pure copper, Scripta Mater. 41 (1999) 755–759.
[15] H. Van Swygenhoven, P. Derlet, Grain-boundary sliding in nanocrystalline fcc metals, Phys. Rev. 64 (2001) 224105–224114.
[16] C. Youngdahl, J. Weertman, R. Hugo, H. Kung, Deformation behavior in nanocrystalline copper, Scripta Mater. 44 (2001) 1475–1478.
[17] J.M. Martin, Antiwear mechanisms of zinc dithiophosphate: a chemical hardness approach, Trib. Lett. 6 (1999) 1–8.